Carbon dioxide uptake by porous organic cages: comparison of high pressure measurements by infrared spectroscopic and manometric techniques

Tom Hasell,[a] Jayne A. Armstrong,[b] Kim E. Jelfs, Feng H. Tay,[c] K. Mark Thomas,[b] Sergei G. Kazarian,[c] and Andrew I. Cooper[a]

Electronic supplementary information:

Materials:

Dichloromethane (DCM, *Fisher*) was used as received. Carbon dioxide (99.9 % pure) was supplied by *BOC* (UK) and used without further purification. **CC1**-**CC3** were synthesised as previously described.[1, 2]

In situ ATR-FTIR spectroscopic measurements:

Apparatus: For the spectroscopic measurements under pressurized CO_2, a heatable Golden Gate™ accessory with a single reflection diamond ATR crystal (*Specac, Ltd*., UK) accessory was used, equipped with a specially designed high-pressure cell, as previously described.[3-6] The Golden Gate™ was used to hold the diamond crystal (ZnSe focusing lenses) with an incident angle of 43° and the deposited cage in the form of a film. The specimen was positioned on top of the crystal mounted in the heating plate connected with a temperature controller. The temperature imposed by the heating plate was to within ±1 K. The high-pressure unit comprised a cell sealed to the tungsten carbide plate of the Golden Gate™ accessory and a syringe pump (*Teledyne 500D, Isco*, USA) imposing the desired pressure, that was measured by a pressure transducer (*Swagelok*, Germany). The accuracy of the pressure measurement was ±0.5 %. A Teflon® O-ring positioned between the cell and the surface of the tungsten carbide plate ensured a good contact between the cell and the surface of the top-plate of the Golden Gate™ accessory avoiding CO_2 leaking. The ATR-IR spectra were collected by means of a Bruker Equinox 55 FT-IR spectrometer with a Mercury– Cadmium–Telluride (MTC) detector. The resolution was 2 cm^{-1}, spectra were obtained with 16 scans and were recorded in 3850–590 cm^{-1} wavenumber range.

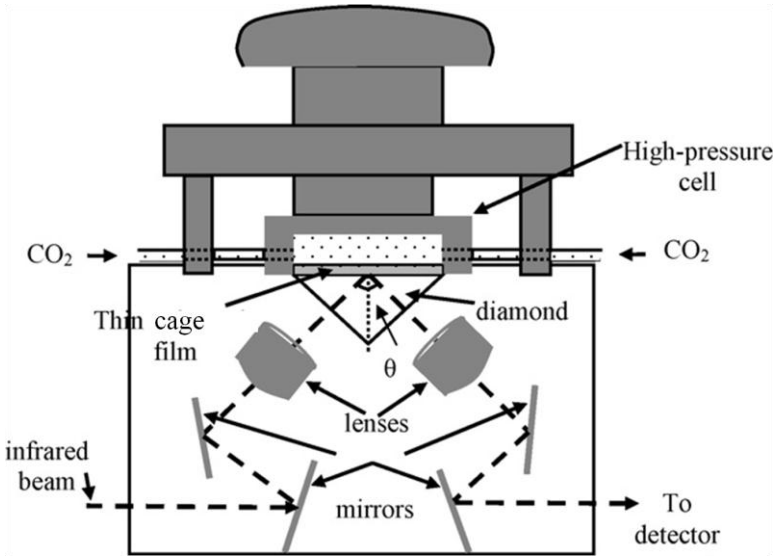

Fig. S1. *Schematic representation of the Golden Gate™ accessory equipped with a specially designed high-pressure cell.*

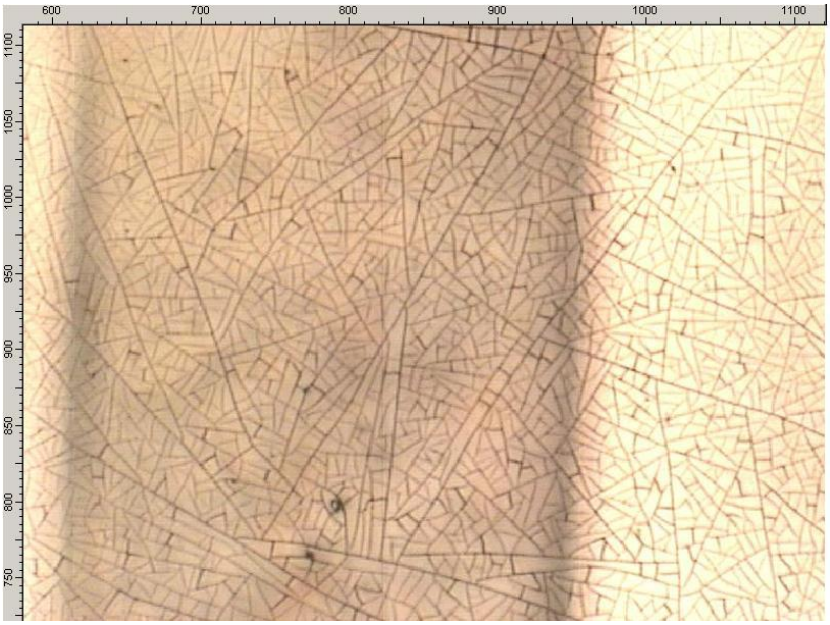

Fig. S2. A representative optical microscope image of a cage film deposited on the ATR crystal, after exposure to high pressure CO_2. Some cracking of the film can be seen to have occurred due to high pressure treatment and heating.

Preparation of the film: Solutions of cage were prepared by dissolving cage powder samples in DCM at 5 mg/mL. This solution was added via a pipette to the surface of the crystal and allowed to evaporate during addition. The solution was added dropwise with care taken to ensure that an even film of cage was produced.

Experimental procedure: The high-pressure cell was first heated to the desired temperature (35 °C) and the spectrum of the cage film, without CO_2, was collected. Thereafter, the CO_2 was introduced into the cell. Next, the outlet valve was closed and the pressure was raised up to the desired value. The cage film was kept at fixed temperature and pressure until equilibrium was reached (typical time ranging from under a minute to several minutes). During this interval spectra were collected at predetermined time: constant absorbance of CO_2 and cage bands indicated the attainment of equilibrium. The analyses were carried out at the pressure range 1–130 bar. Spectra of pure CO_2 in the same conditions were recorded as well. Solely the CO_2 dissolved in the cage film can be detected without contribution of the bulk CO_2 above the film, owing to the fact that the beam penetration depth (a few micrometers) was much smaller than the film thickness of cage materials.

Gravimetric Measurements:

Low temperature adsorption characteristics were investigated using an Intelligent Gravimetric Analyzer (IGA) supplied by Hiden Isochema Ltd., Warrington, UK. The IGA system is an ultra-high vacuum (UHV) system comprising of a fully computer controlled microbalance and, pressure admit and temperature regulation systems. The mass was recorded using a microbalance and the temperature and pressure were computer controlled. The sample was outgassed to a constant weight, at $< 10^{-6}$ Pa, at 383 K. Three pressure transducers with individual pressure ranges of 0-0.2 kPa, 0-10 kPa and 0-100 kPa were used to control the admitted gas/vapor pressure. The set pressure value was maintained by computer control during the course of the experiment with an accuracy of ±0.02 of the pressure range. The sample temperature was achieved using a solid carbon dioxide/acetone bath and recorded using a thermocouple located 5 mm from the sample The equilibrium uptake value was determined as being 99.9 % of the predicted value, calculated in real time using the mass uptake profile.

Manometric Measurements:

High pressure carbon dioxide isotherms were measured on the Hiden Isochema Intelligent Manometric Instrument (IMI). The sample mass used was ~ 300 mg. The density of the sample was measured using helium pycnometry. Equilibration relaxation kinetics were monitored using a computer algorithm with calculations carried out in real time with equilibrium uptake value

determined when 99.9 % of the predicted value was achieved. Typical equilibration times were < 1 h. The sample temperature was controlled to better than ± 0.1 K. Surface excess amounts were calculated using the equation of state.[7] The repeatability of the surface excess isotherm points averaged ± 0.6 %.

The absolute isotherms were calculated using crystallographic data and the following equation:

$$n_{ex} = n_{abs} - V_{pore} * \rho_{gas} \qquad (1)$$

Where n_{ex} is the surface excess determined experimentally, n_{abs} is the absolute adsorption, and the V_{pore}*ρ_{gas} terms defines the 'free gas' present in the pores – where ρ_{gas} is the density of the gas phase and V_{pore} is the crystallographic pore volume determined using PLATON. The density of the gas phase was obtained using REFPROP.
Saturated vapor pressures were calculated using the Antoine equation:

$$\log p^0 = A - \frac{B}{T + C} \qquad (2)$$

Where p^0 is the saturated vapor pressure (Torr), T is the temperature (K), and A, B, and C are adsorbate dependent constants. The parameters used for each adsorptive are as follows: carbon dioxide (77 – 303 K) (A) 7.81024, (B) 995.705, (C) 293.475

Modelling simulations:

The adsorption isotherms of **CC1α**, **CC1β**, **CC2** and **CC3** were simulated using CSFF,[8] a forcefield based upon PCFF[9] that we have previously parameterised specifically for gas diffusion in our organic cage systems. We use partial charges from the forcefield and note that we have not specifically reparameterised the intermolecular interactions between the gas molecules and the organic host, as has been done for other studies of accurate gas uptake on porous molecular materials.[10] The loadings were calculated in fixed cells, where supercells were used when required to ensure the minimum cell length was 20 Å (**CC1α**: 2 x 2 x 1; **CC1β**: 1 x 1 x 2; **CC2**: 2 x 2 x 2 and **CC3**: 1 x 1 x 1). The Single Crystal X-ray Diffraction (SC-XRD) structures were used and because **CC2** has positional disorder of the methyl positions on the vertices, these were randomised over the supercell. The Sorption module for Grand Canonical Monte Carlo (GCMC) calculations within Accelrys' Materials Studio 5.0 package was used. Each simulation was carried out at a temperature of 303 K and had an equilibration period of 15-million steps and a production period of 10-million steps. The sorption positions were sampled every 1000 steps. Connolly surface areas were calculated in Materials Studio using a probe radius of 1.6 Å for CO_2[11] and a grid spacing of 0.15 Å.

Theory of calculating CO_2 adsorption from spectral adsorption:

Briefly, in the ATR-FTIR spectroscopic technique the beam of infrared radiation traverses a pyramidal crystal of relatively high refractive index (in this case 2.42) and internally reflects from the crystal surface at an angle of incidence, θ, creating an evanescent wave projected orthogonally into the specimen positioned in intimate contact with the ATR crystal. The penetration depth (d_p) is given by:[3, 5]

$$d_p = \frac{\lambda}{2\pi\sqrt{(n_1^2 \sin^2\theta - n_2^2)}} \qquad (3)$$

where, λ is the wavelength of the incident light, θ is the incident angle, n_1 and n_2 are the refractive indexes of the ATR-IR crystal and the sample, respectively. In order to apply the Beer-Lambert law, the path length that would give the same absorbance in transmission as that obtained in an ATR-IR

experiment must be determined. For polarised light this can be calculated based on the refractive index of the crystal, the refractive index of the sample, the angle of incidence and the wavelength of the incident beam.[4, 5] This is termed the effective thickness, d_e, for polarised light, and $d_{e,u}$ for unpolarised light, which is taken as the average effective thickness of parallel and perpendicular polarised light.

The solubility of CO_2 in the cage film was calculated from the absorbance of the asymmetric stretching vibrational band of CO_2 at 2333 cm^{-1}. To measure the solubility of CO_2, the Lambert–Beer law, which expresses the relation between the absorbance, A, the concentration, c, the effective thickness, $d_{e,u}$, and the absorptivity, ε, was used:

$$A = \varepsilon c d_{e,u} \qquad (4)$$

The input data necessary to calculate these parameters are: diamond (ATR material) refractive index = 2.42; sample refractive index taken to be = 1.33 (non-trivial to determine, so approximated to that of water); angle of incidence = 43°; wavelength = 2333 cm^{-1}. The absorbance of the 2333 cm^{-1} band was quantified by measuring the height of the relevant peak. As molar absorptivity of high-pressure CO_2 the value of 1.0×10^6 cm^2 mol^{-1} was used.[12] By comparing the observed CO_2 concentration with the density of **CC2** and **CC3** (0.874 g cm^{-3} and 1.051 g cm^{-3} respectively), the uptake of CO_2 into the cage film, in mmol g^{-1}, can be calculated as a function of CO_2 pressure or density.

The gaseous and adsorbed CO_2 bands are sufficiently shifted to be easily resolved. If there is no significant contribution from gaseous CO_2, as is normally the case, then no correction needs to be made. However, if there is some contribution from gaseous CO_2, then this can be subtracted from the spectrum to give just the signal for the adsorbed CO_2. As the IR penetration depth is much thinner than the thickness of the film, it is unsurprising that there is not normally any significant contribution from gaseous CO_2 – unless there are cracks present in the films.

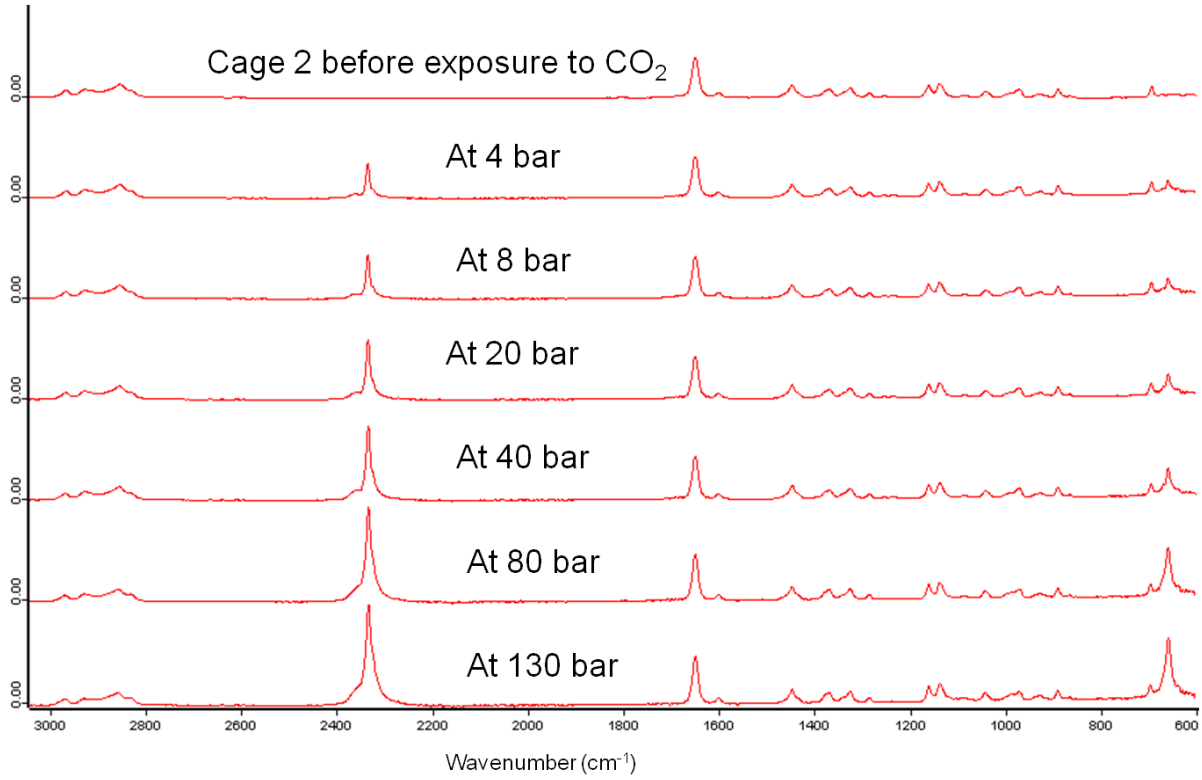

Fig. S3. ATR-FTIR spectra of **CC2**. The spectra are stacked to show the effect of the increase in CO_2 pressure into the cell.

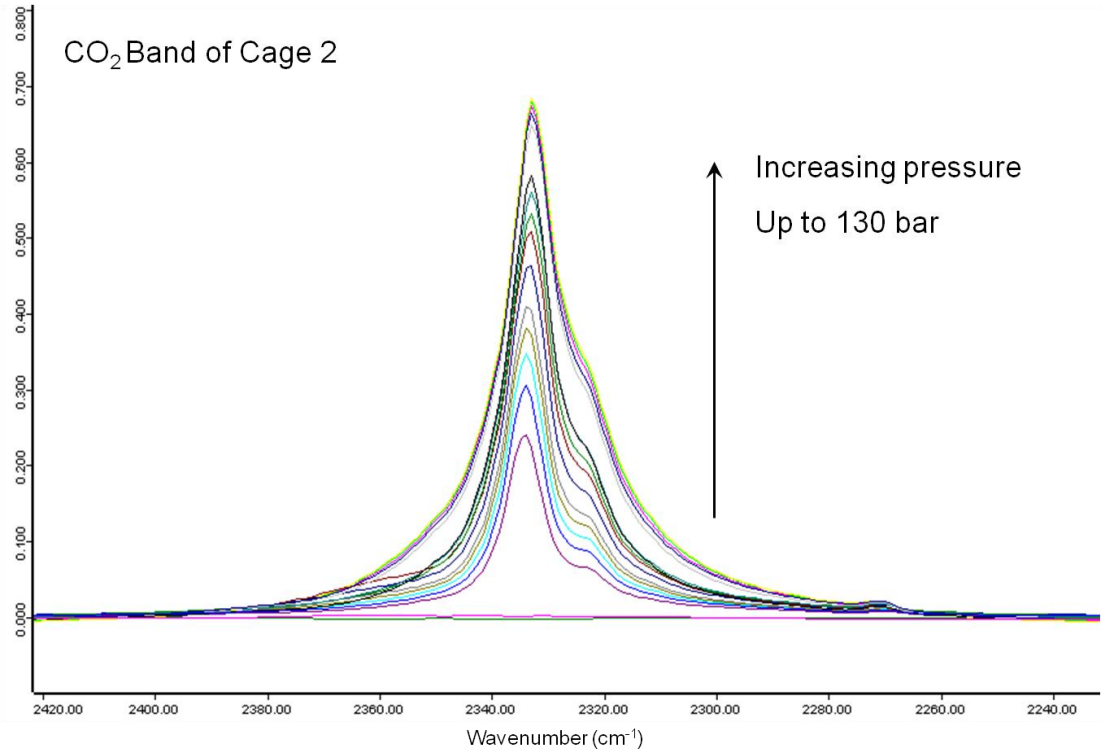

Fig. S4. Absorbance of the 2333 cm^{-1} band of CO_2 in **CC2** in the 0-130 bar pressure range.

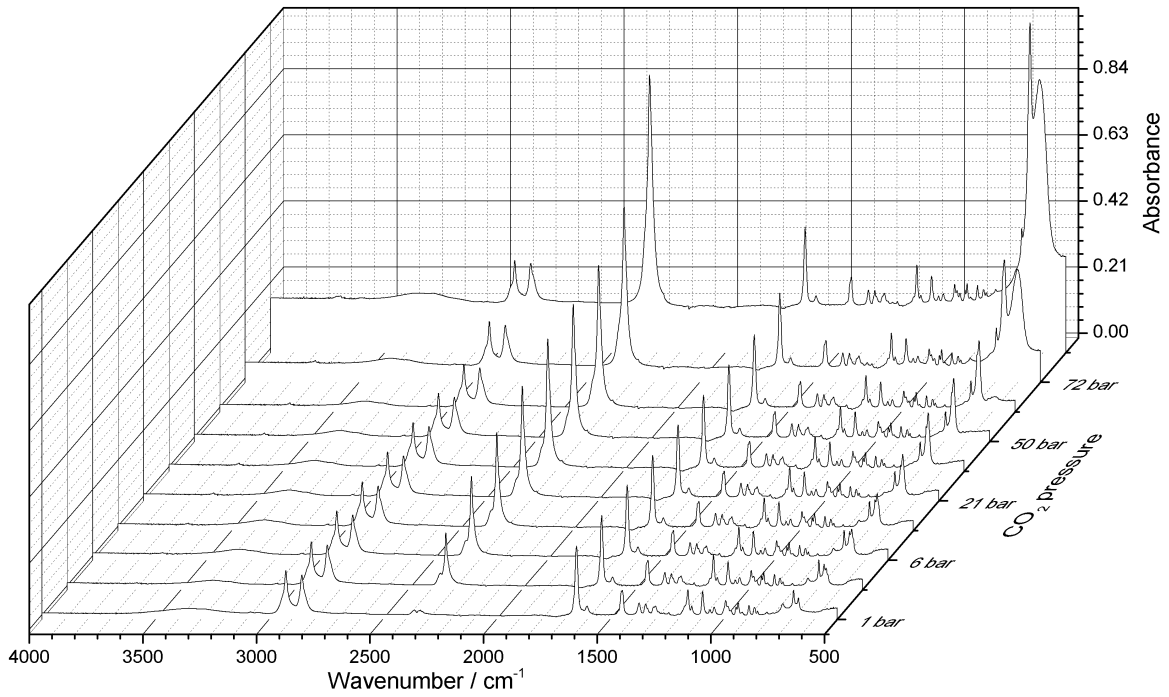

Fig. S5. ATR-FTIR spectra of **CC3**. The spectra are shown as a waterfall plot to display the effect of the increase in CO_2 pressure into the cell.

High Pressure Adsorption:

The difference between surface excess and absolute isotherms becomes significant as pressure increases and this is particularly important in the context of high pressure supercritical gas adsorption. Manometric and gravimetric methods provide measurements of the surface excess and the absolute isotherm can be calculated for crystalline materials using the crystallographic pore volume. The measurement of the absolute isotherms for amorphous materials is much more problematic.

The surface excess is the experimentally measured parameter and is the amount adsorbed, which exceeds gas phase density. The amount corresponding to the adsorbed phase layer is described by the absolute isotherm.

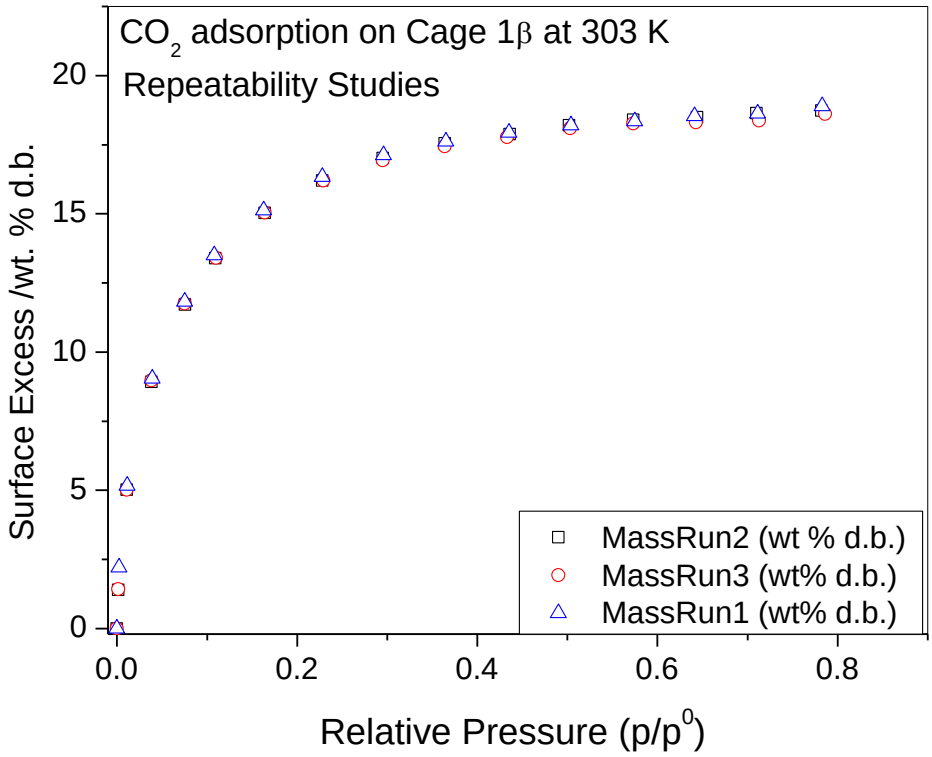

Fig. S6. Manometrically derived CO_2 adsorption onto **CC1β**, at 303 K, as a function of pressure. Data are shown as open squares (surface excess), closed squares (absolute), and open triangles (free gas).

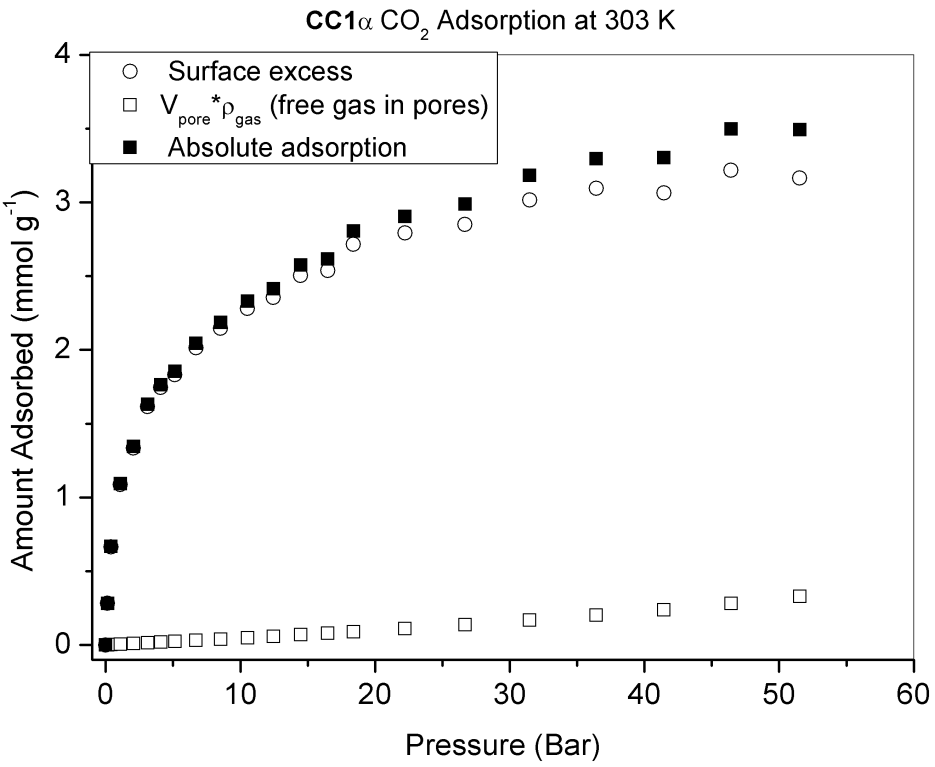

Fig. S7. CO_2 adsorption isotherms for **CC1α** (303 K) as a function of pressure. The manometrically-derived surface excess is shown (open circles), compared to the calculated free gas present in the pores (open squares) and the absolute isotherm (closed squares).

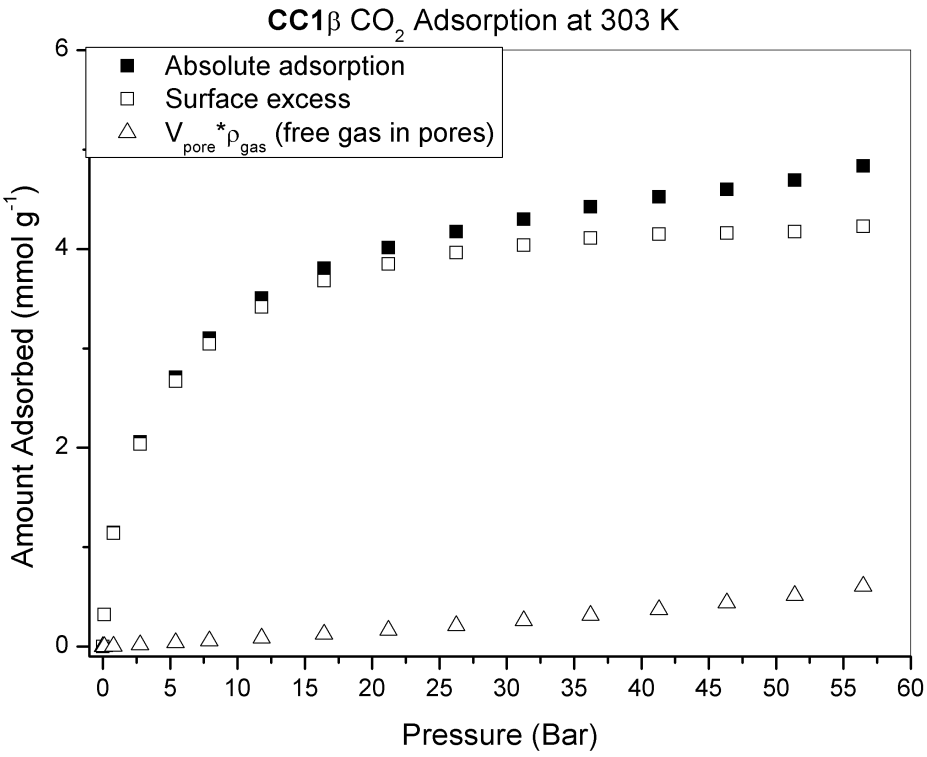

Fig. S8. CO_2 adsorption isotherms for **CC1β** (303 K) as a function of pressure. The manometrically-derived surface excess is shown (open squares), compared to the calculated free gas present in the pores (open triangles) and the absolute isotherm (closed squares).

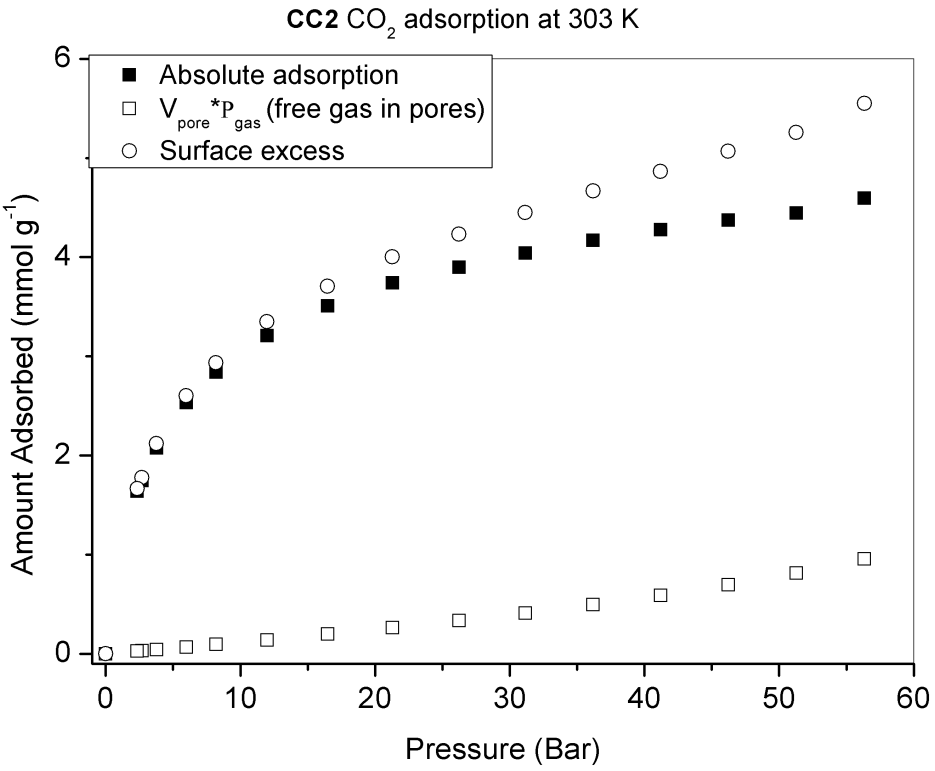

Fig. S9. CO_2 adsorption isotherms for **CC2** (303 K) as a function of pressure. The manometrically-derived surface excess is shown (open circles), compared to the calculated free gas present in the pores (open squares) and the absolute isotherm (closed squares).

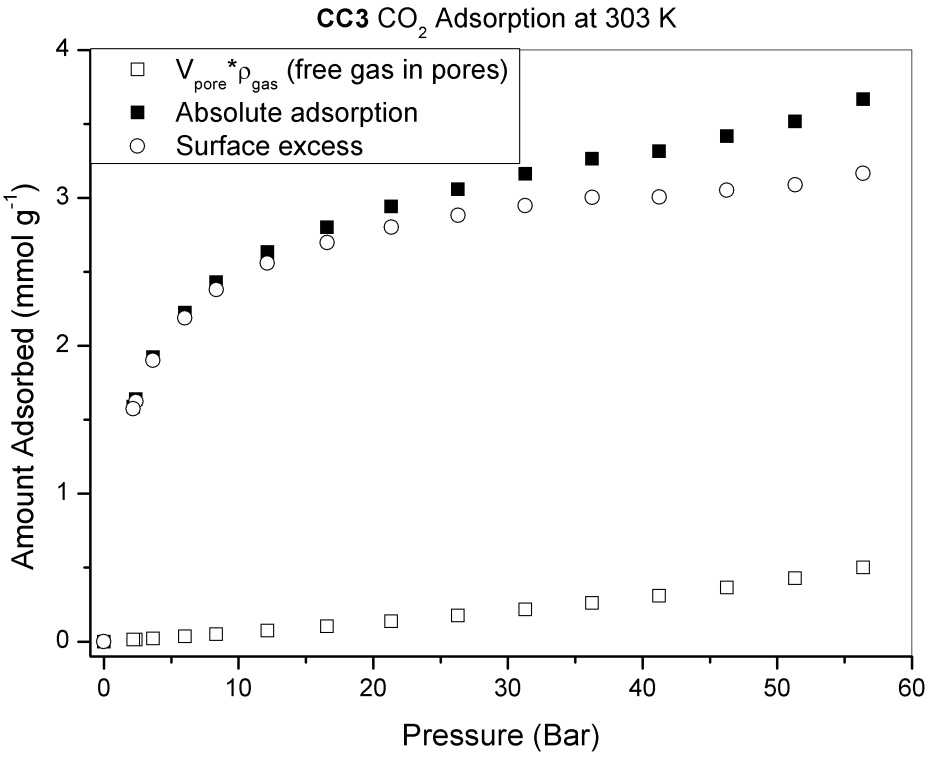

Fig. S10. CO_2 adsorption isotherms for **CC3** (303 K) as a function of pressure. The manometrically-derived surface excess is shown (open circles), compared to the calculated free gas present in the pores (open squares) and the absolute isotherm (closed squares).

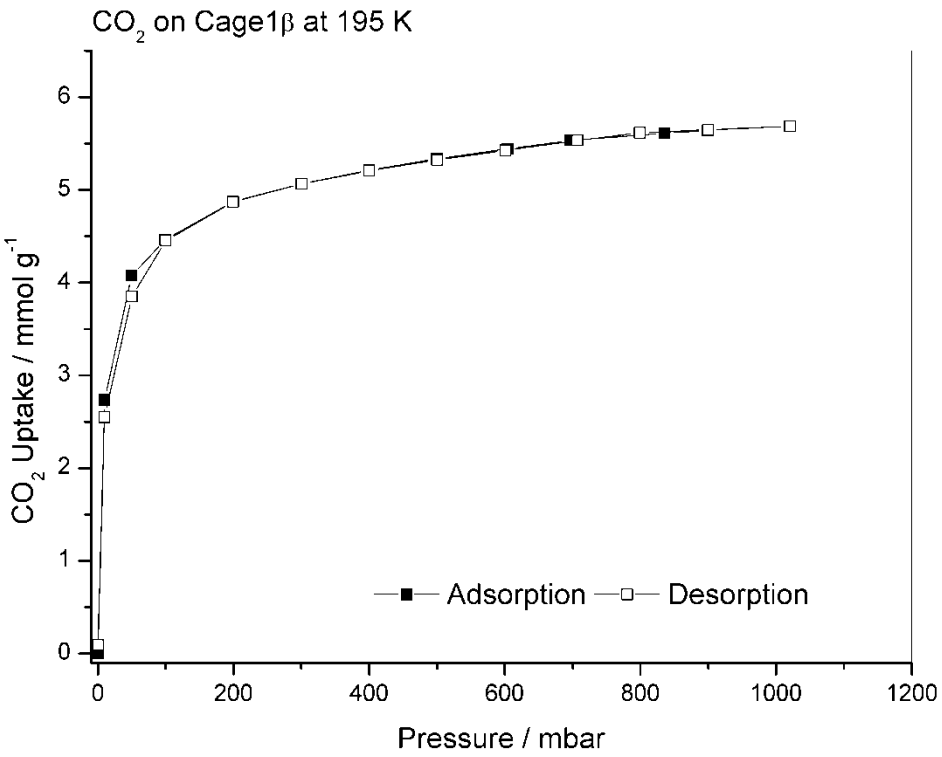

Fig. S11. Manometrically derived CO_2 adsorption onto **CC1β**, at 195 K, as a function of pressure. Data are shown as closed squares (adsorption), and open squares (desorption).

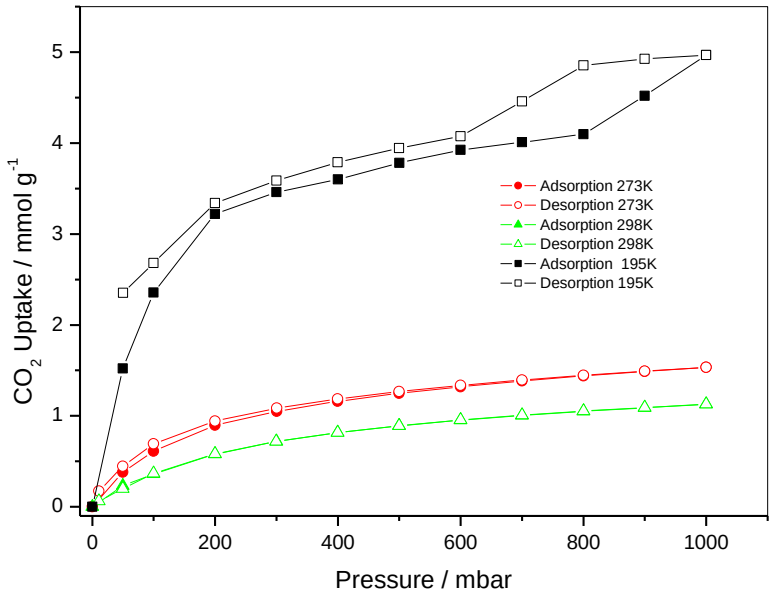

Fig. S12. Manometrically derived CO_2 adsorption onto **CC1α**, at 195, 298, and 273 K, as a function of pressure. Data are shown as closed squares (adsorption), and open squares (desorption).

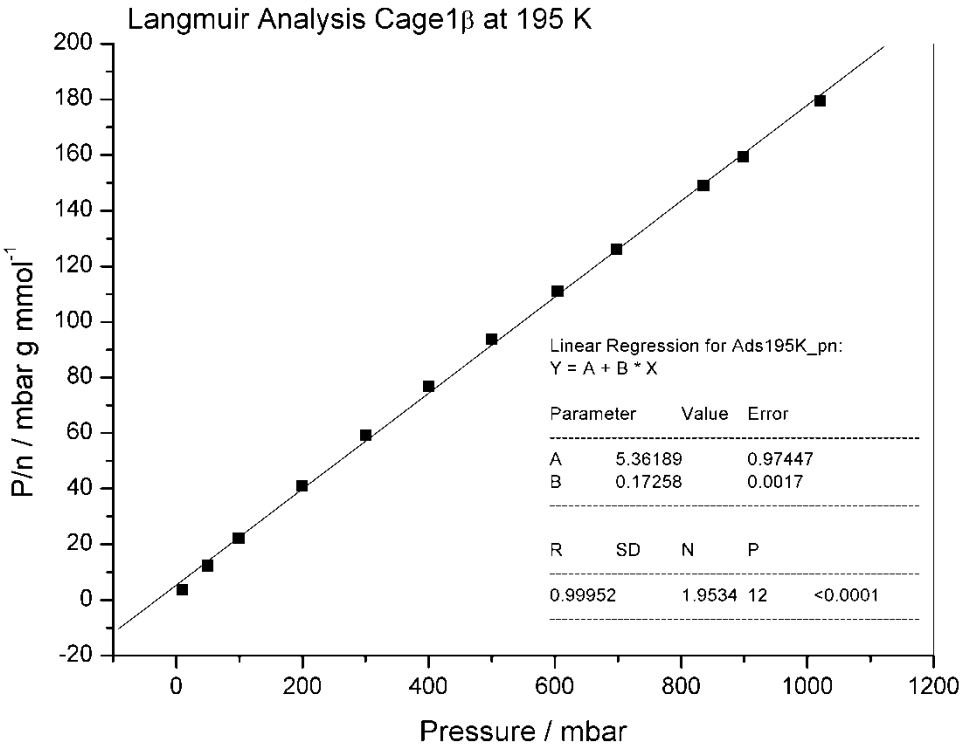

Fig. S13. Langmuir analysis based on the manometric CO_2 adsorption onto **CC1β**, at 195 K, as a function of pressure.

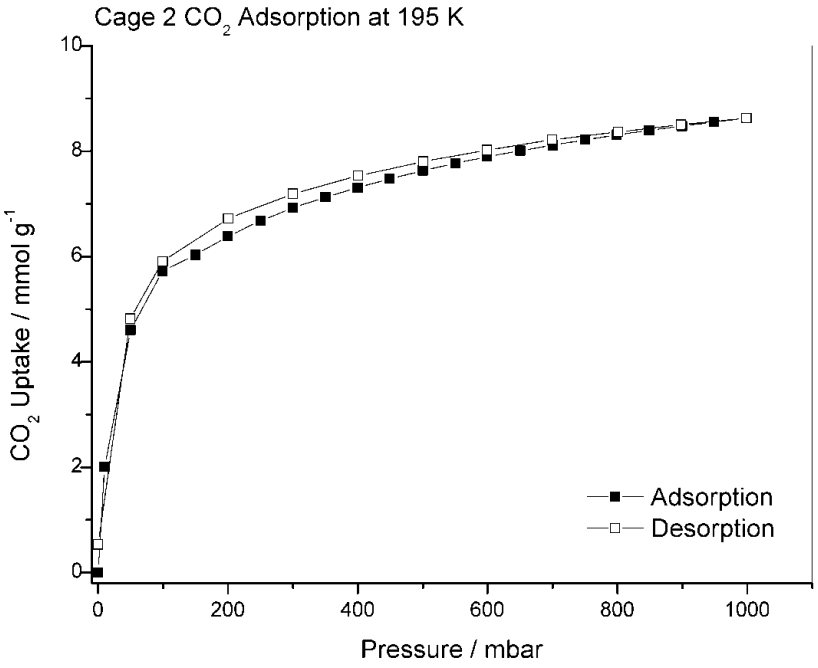

Fig. S14. Manometrically derived CO_2 adsorption onto **CC2**, at 195 K, as a function of pressure. Data are shown as closed squares (adsorption), and open squares (desorption).

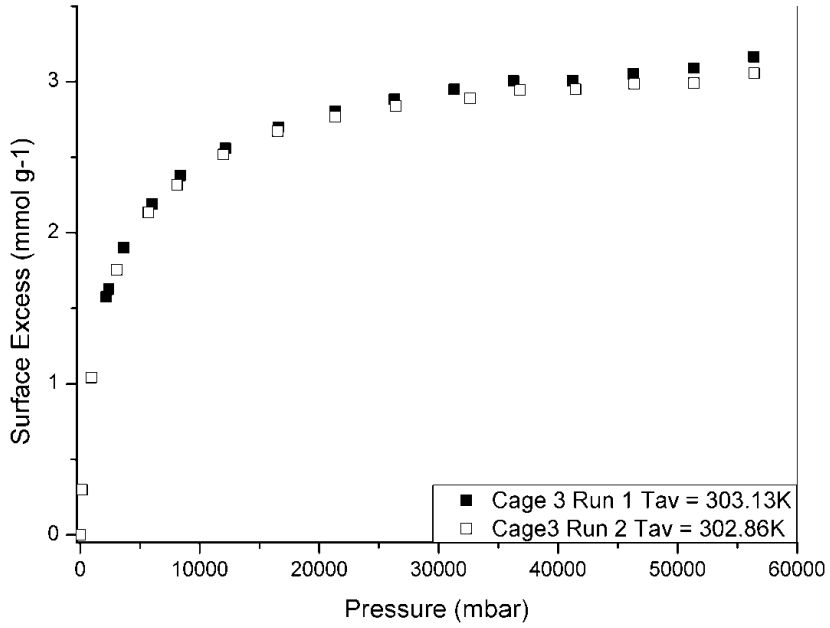

Fig. S15. Manometrically derived CO_2 adsorption onto **CC3**, at 303 K, as a function of pressure. Data are shown as closed squares and open squares for two repeat runs.

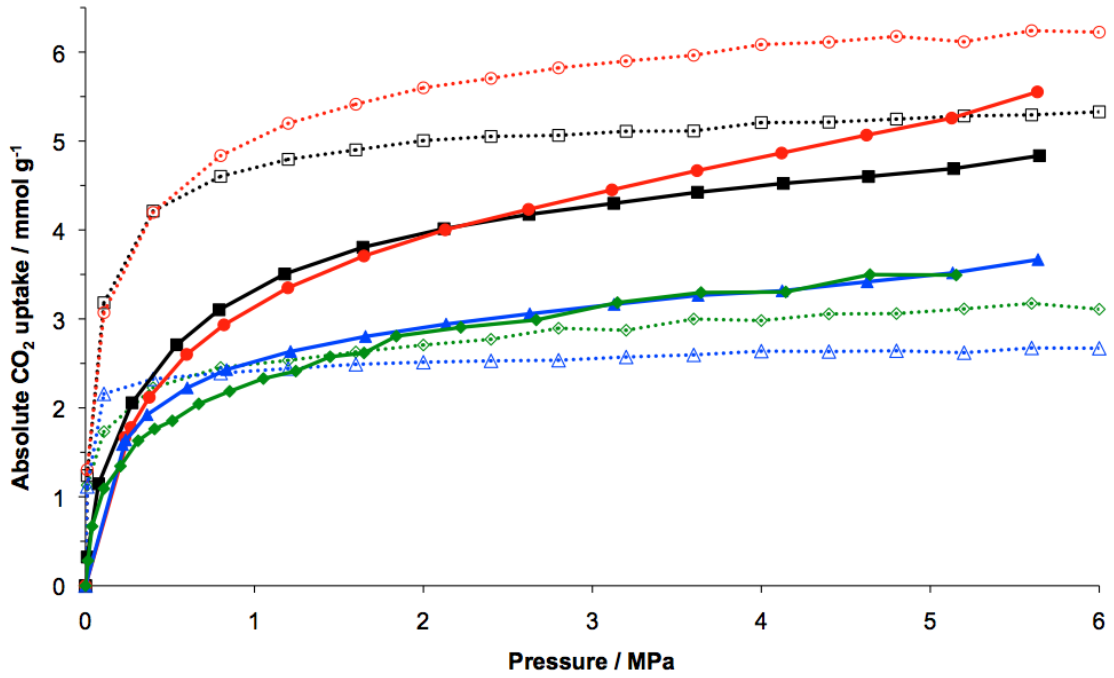

Fig. S16. A comparison of simulated and experimental isotherms for CO_2 at 303 K for **CC1α** (green diamonds), **CC1β** (black squares), **CC2** (red circles), and **CC3** (blue triangles). The experimental results are shown as the absolute isotherm derived from manometric measurements (closed symbols) against the simulated absolute isotherms (open symbols, dotted lines). Discrepency of the simulated to the experimental results, at the highest experimentally measured pressure, are as follows: **CC1α:** -10.9 %, **CC1β**: +9.5 %, **CC2:** +12.4 %, and **CC3:** -27.1 %. This level of agreement is reasonable for a molecular material.[10]

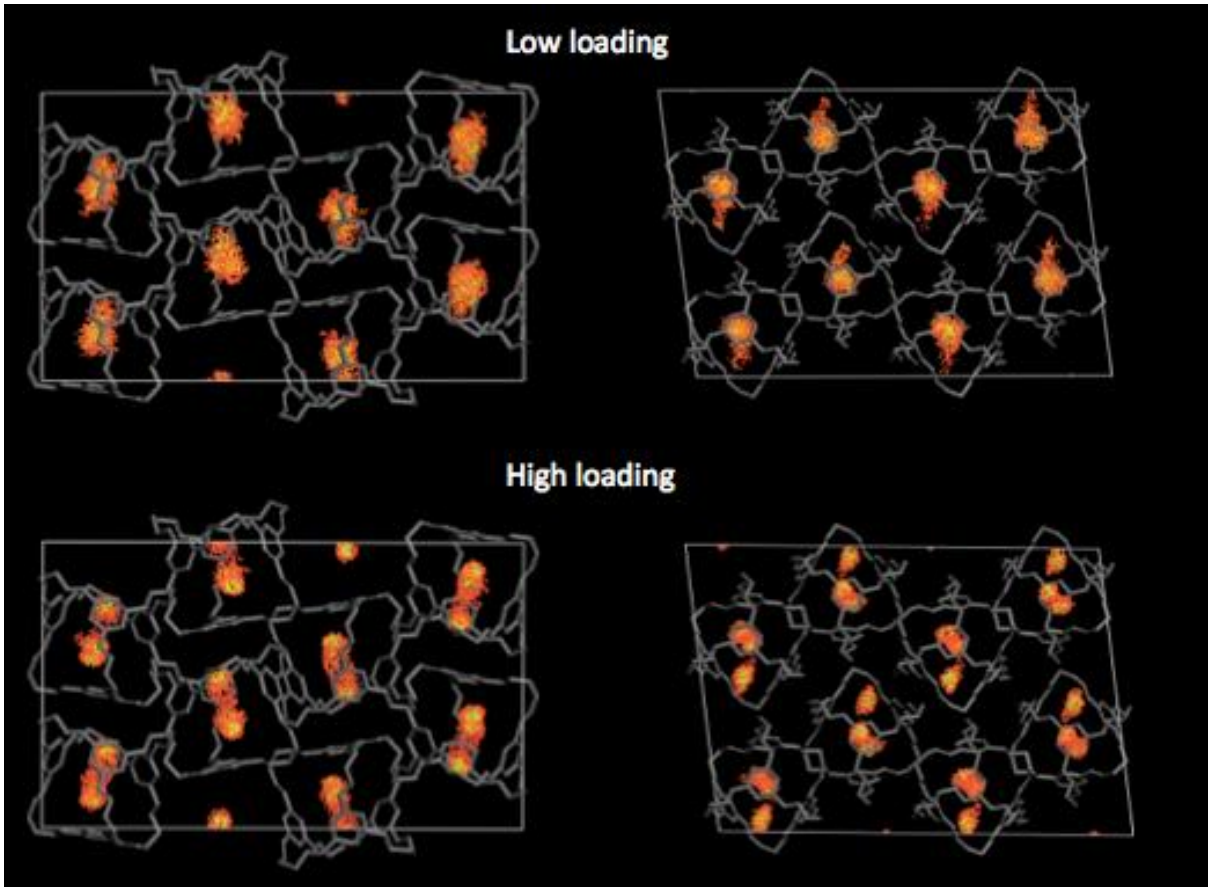

Fig S17: The CO_2 density maps showing the preferred sorption sites over the simulation for **CC1α**, as sampled over the period of the GCMC simulation. Brighter points (yellow) were sampled more frequently. Two perpendicular views are shown at each loading level, low leading corresponds to 0.1 MPa and high loading corresponds to 6 MPa.

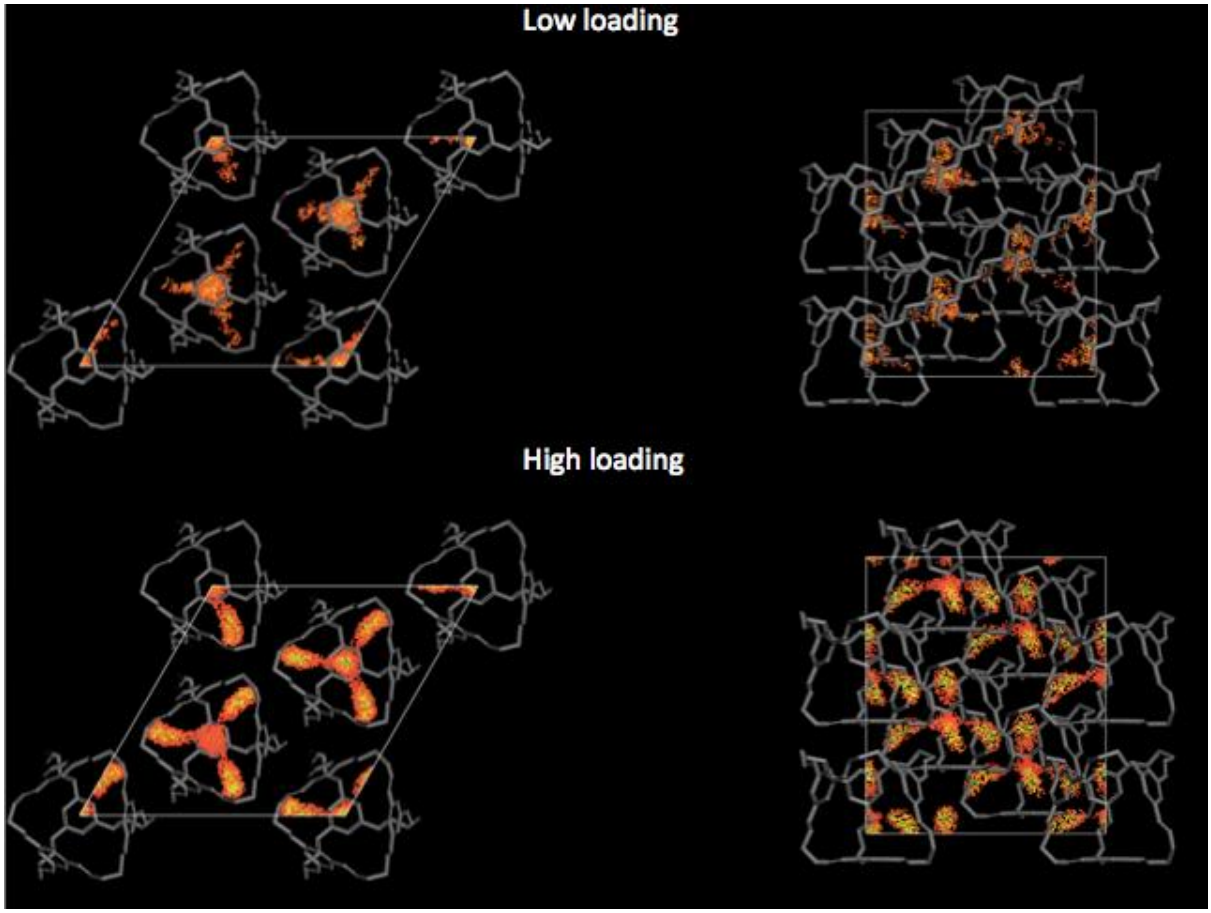

Fig S18: The CO_2 density maps showing the preferred sorption sites over the simulation for **CC1β**, as sampled over the period of the GCMC simulation. Brighter points (yellow) were sampled more frequently. Two perpendicular views are shown at each loading level, low leading corresponds to 0.1 MPa and high loading corresponds to 6 MPa.

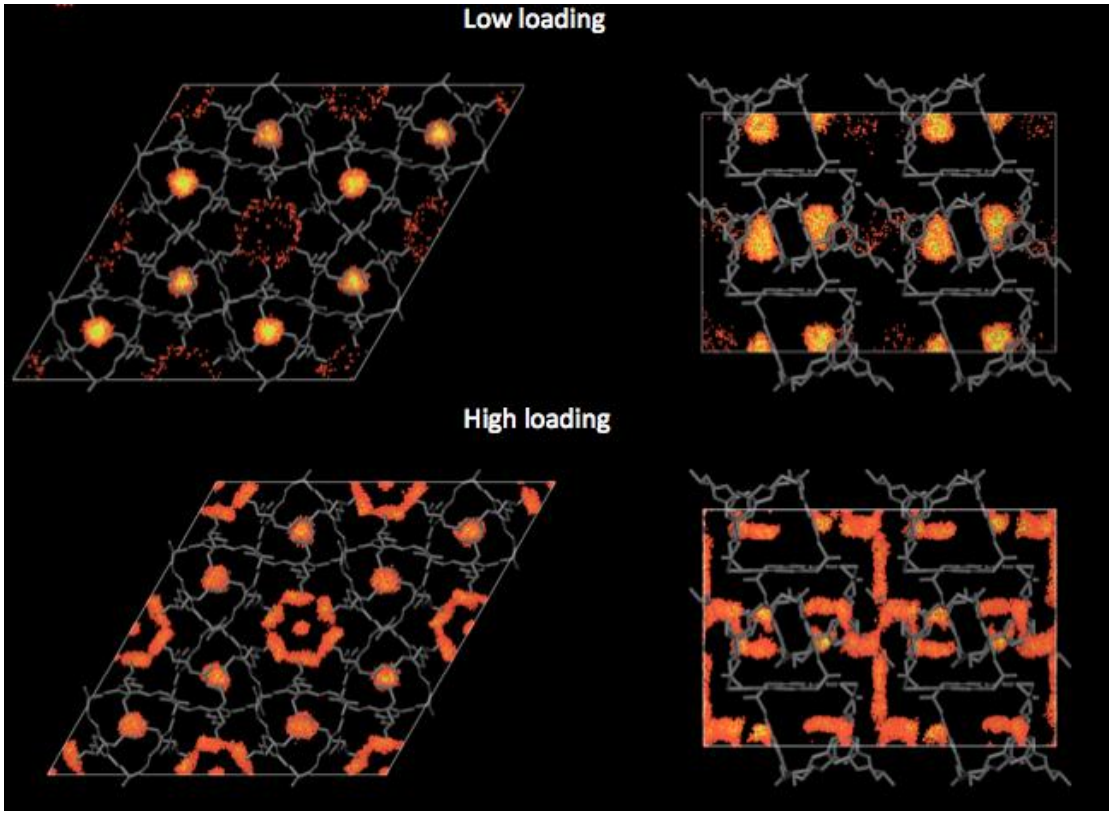

Fig S19: The CO_2 density maps showing the preferred sorption sites over the simulation for **CC2**, as sampled over the period of the GCMC simulation. Brighter points (yellow) were sampled more frequently. Two perpendicular views are shown at each loading level, low leading corresponds to 0.1 MPa and high loading corresponds to 6 MPa. The left hand view is shown down the 1-D channel.

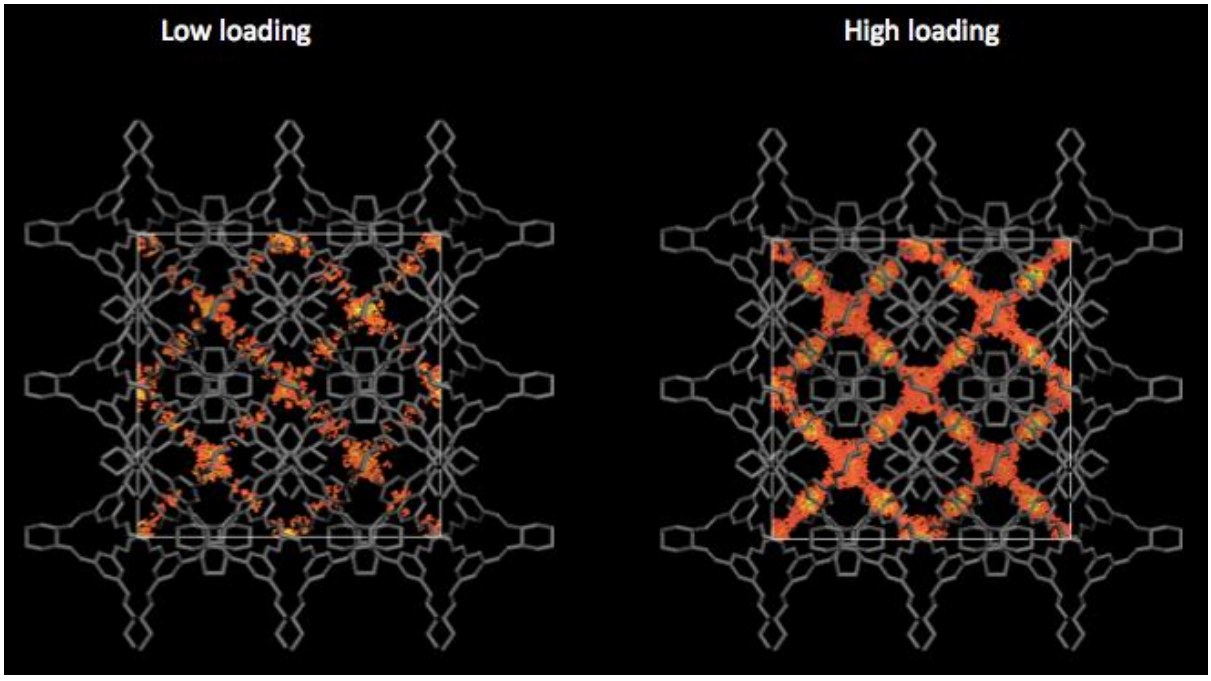

Fig S20: The CO_2 density maps showing the preferred sorption sites over the simulation for **CC3**, as sampled over the period of the GCMC simulation. Brighter points (yellow) were sampled more frequently. Low leading corresponds to 0.1 MPa and high loading corresponds to 6 MPa.

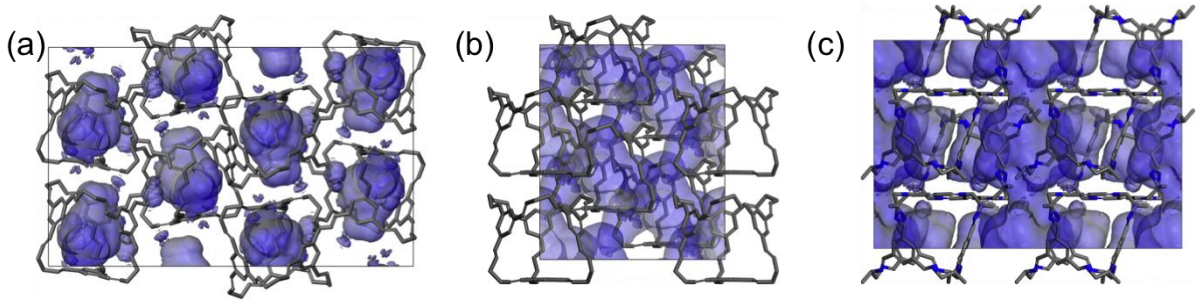

Fig S21: Views of the Connolly surface area shown in blue, as calculated with a CO_2 probe of radius 1.6 Å[11] in Materials Studio. These views are perpendicular to those shown in Fig. 7 for (a) 2 x 1 x 1 supercell of **CC1α** (b) **CC1β** and (c) 2 x 2 x 2 supercell of **CC2**.

1. T. Hasell, S. Y. Chong, K. E. Jelfs, D. J. Adams and A. I. Cooper, *Journal of the American Chemical Society*, 2012, **134**, 588-598.
2. D. P. Lydon, N. L. Campbell, D. J. Adams and A. I. Cooper, *Synth. Commun.*, 2011, **41**, 2146-2151.
3. I. Pasquali, J. M. Andanson, S. G. Kazarian and R. Bettini, *J. Supercrit. Fluids*, 2008, **45**, 384-390.
4. A. R. C. Duarte, L. E. Anderson, C. M. M. Duarte and S. G. Kazarian, *Journal of Supercritical Fluids*, 2005, **36**, 160-165.
5. N. M. B. Flichy, S. G. Kazarian, C. J. Lawrence and B. J. Briscoe, *J. Phys. Chem. B*, 2002, **106**, 754-759.
6. S. G. Kazarian, *Macromolecular Symposia*, 2002, **184**, 215-228.
7. *NIST Standard Reference Database 23. NIST Reference Fluid Thermodynamic and Transport Properties—REFPROP Version 8*
8. D. Holden, K. E. Jelfs, A. I. Cooper, A. Trewin and D. J. Willock, *Journal of Physical Chemistry C*, 2012, **116**, 16639-16651.
9. H. Sun, *Macromolecules*, 1995, **28**, 701-712.
10. W. Li, S. Grimme, H. Krieg, J. Moellmann and J. Zhang, *Journal of Physical Chemistry C*, 2012, **116**, 8865-8871.
11. C. E. Webster, R. S. Drago and M. C. Zerner, *Journal of the American Chemical Society*, 1998, **120**, 5509-5516.
12. P. G. Maiella, J. W. Schoppelrei and T. B. Brill, *Appl. Spectrosc.*, 1999, **53**, 351-355.